

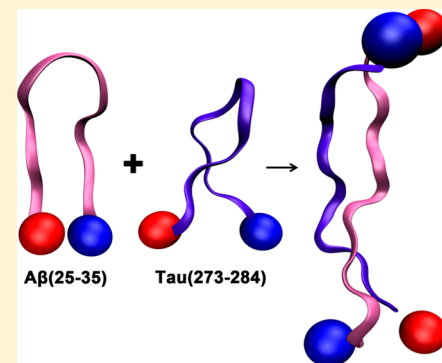
# Interactions between Amyloid- $\beta$ and Tau Fragments Promote Aberrant Aggregates: Implications for Amyloid Toxicity

Thanh D. Do,<sup>†</sup> Nicholas J. Economou,<sup>†</sup> Ali Chamas,<sup>†</sup> Steven K. Buratto,<sup>†</sup> Joan-Emma Shea,<sup>†,‡</sup> and Michael T. Bowers\*,<sup>†</sup>

<sup>†</sup>Department of Chemistry and Biochemistry and <sup>‡</sup>Department of Physics, University of California, Santa Barbara, California 93106, United States

## S Supporting Information

**ABSTRACT:** We have investigated at the oligomeric level interactions between A $\beta$ (25–35) and Tau(273–284), two important fragments of the amyloid- $\beta$  and Tau proteins, implicated in Alzheimer's disease. We are able to directly observe the coaggregation of these two peptides by probing the conformations of early heterooligomers and the macroscopic morphologies of the aggregates. Ion-mobility experiment and theoretical modeling indicate that the interactions of the two fragments affect the self-assembly processes of both peptides. Tau(273–284) shows a high affinity to form heterooligomers with existing A $\beta$ (25–35) monomer and oligomers in solution. The configurations and characteristics of the heterooligomers are determined by whether the population of A $\beta$ (25–35) or Tau(273–284) is dominant. As a result, two types of aggregates are observed in the mixture with distinct morphologies and dimensions from those of pure A $\beta$ (25–35) fibrils. The incorporation of some Tau into  $\beta$ -rich A $\beta$ (25–35) oligomers reduces the aggregation propensity of A $\beta$ (25–35) but does not fully abolish fibril formation. On the other hand, by forming complexes with A $\beta$ (25–35), Tau monomers and dimers can advance to larger oligomers and form granular aggregates. These heterooligomers may contribute to toxicity through loss of normal function of Tau or inherent toxicity of the aggregates themselves.



## INTRODUCTION

Senile plaques of amyloid- $\beta$  (A $\beta$ ) and neurofibrillary tangles (NFT) of Tau are pathophysiological markers of Alzheimer's disease (AD). Tau proteins include six different intracellular, intrinsically disordered isoforms consisting of two functional domains. The projection domain mediates interactions of microtubules with neural plasma membrane and cytoskeletal elements and is involved in signal transduction, while the Tau microtubule binding pseudorepeat domain (MTBR) regulates microtubule assembly from tubulin (for a comprehensive review, see ref 1). Aggregation of Tau into NFT is promoted in cases of hyperphosphorylation or deficiency in dephosphorylation.<sup>1–3</sup> More than 37 mutations of Tau isoforms have been shown to induce neurodegenerative diseases (e.g., frontotemporal dementia);<sup>3,4</sup> however, there are no Tau mutations directly linked to any known familial form AD. While a "loss of function" hypothesis is often invoked to explain the role of Tau aggregation in AD, the latter does not fully account for the etiology of the disease, and does not address the role of A $\beta$  in AD, or its possible interaction with Tau.<sup>5</sup>

Unlike Tau which resides in the neurons, the A $\beta$  peptide is produced in the extracellular space from the proteolytic cleavage of a large transmembrane amyloid  $\beta$ -protein precursor protein (APP). An amyloid cascade hypothesis has been proposed that stipulates that AD is caused by the aggregation of A $\beta$ ,<sup>6</sup> with  $\beta$ -rich toxic oligomers<sup>6,7</sup> or fibrillar aggregates<sup>8</sup>

signaling cell apoptosis or decreasing synaptic plasticity. However, this hypothesis has been challenged given the lack of strong correlation between the amount of A $\beta$  produced, or senile plaques deposited, and neuronal loss or cognitive impairment.<sup>9,10</sup> The observation that A $\beta$  monomers or soluble oligomers permeate cell membranes<sup>11,12</sup> and form highly functional multimeric aggregates<sup>6</sup> capable of interfering with normal cellular activities is offering a new research direction in AD. Yet another hypothesis, and the one that we will focus on in this work, is that the interaction of A $\beta$  and Tau may be significant in AD. Indeed, while the A $\beta$  peptide is produced in the extracellular space, soluble A $\beta$  oligomers have been shown to exist in the intracellular space as well<sup>13</sup> and interact with a variety of proteins<sup>14</sup> including Tau.<sup>15–21</sup> Exposure of Tau to A $\beta$  oligomers<sup>22</sup> could lead to loss of microtubule integrity,<sup>15</sup> formation of new, insoluble aggregates,<sup>23</sup> or an enhancement of NFT formation.<sup>8</sup> Tau has been shown to induce A $\beta$  toxicity in hippocampal neurons,<sup>24</sup> while A $\beta$ -mediated Tau phosphorylation has been discovered in both hippocampal and cholinergic neurons.<sup>19,25–27</sup>

The full length A $\beta$  is a 39–43-residue peptide with A $\beta$ (1–40) and A $\beta$ (1–42) being the two most abundant isoforms. The

Received: June 24, 2014

Revised: August 23, 2014

Published: August 25, 2014

full length Tau, depending on its isoforms, can be as long as 400 residues, and studying complexes of  $\text{A}\beta$  and Tau poses a real challenge, both from an experimental and computational standpoint. We then turn in this work to the study of a model system that captures the essential features of  $\text{A}\beta$  and Tau assembly. We use a combination of ion-mobility mass spectrometry (IM-MS), atomic force microscopy (AFM), and computational modeling to investigate the interactions between an  $\text{A}\beta$  and a Tau fragment:  $\text{A}\beta(25–35)$  and Tau(273–284). These two peptide fragments contain important regions of the full  $\text{A}\beta$  and Tau proteins, and we and others have studied early oligomer conformations and aggregation propensities of both peptides.<sup>28–33</sup>  $\text{A}\beta(25–35)$  is an amphipathic peptide with similar aggregation propensity and toxicity to the full length  $\text{A}\beta(1–42)$ .<sup>34,35</sup> Takashima et al.<sup>27</sup> have shown that embryonic rat hippocampal neurons undergo progressive degeneration and that Tau phosphorylation is enhanced after exposure to  $\text{A}\beta(25–35)$ , similar to the result obtained with  $\text{A}\beta(1–40)$  by Busciglio and co-workers.<sup>25</sup> Tau(273–284) is in the second repeat (R2) of MTBR and encompasses the PHF6\* hexapeptide (VQIINK), one of the two hexapeptides known to play an important role in Tau aggregation.<sup>36–39</sup> It has also been shown experimentally that Tau binds between the middle and C-terminal regions of  $\text{A}\beta(1–42)$  (the region of APP inserted into the cell membrane).<sup>23</sup> A recent theoretical work by Nussinov and co-workers also suggests that  $\text{A}\beta$  oligomers interact more strongly with R2 of MTBR than R3 or R4.<sup>40</sup> Although R2 appears in some but not all Tau isoforms (encoded only by exon 10 of the MAPT protein), changing the ratio of four-repeat Tau to three-repeat Tau is sufficient to cause serious degeneration in microtubule assembly.<sup>41</sup>

Of note is that both peptides contain a hydrophobic stretch of six-residue sequence, i.e., PHF6\* in Tau(273–284) and GAIIGL from  $\text{A}\beta(25–35)$ . These two hexapeptides have been shown to adopt steric zipper motifs that facilitate amyloid fibril formation.<sup>36,42,43</sup> The sequences of the fragments are shown in Figure 1.

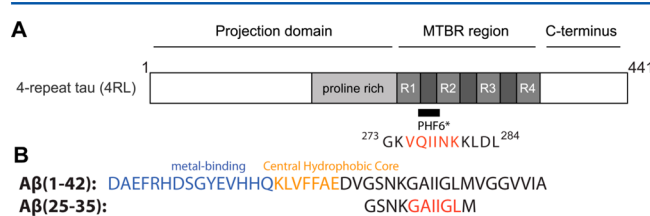


**Figure 1.** (A) Full length four-repeat Tau and location of PHF6\* and the Tau(273–284) construct used in this study (see Larini et al.<sup>30</sup> Adapted in part from ref 30. Copyright 2013 Royal Society of Chemistry.). The longest Tau isoforms contain either three or four imperfect repeats in the microtubule-binding pseudorepeat domain (MTBR). (B) Full length  $\text{A}\beta(1–42)$  with different regions and the peptide sequence of  $\text{A}\beta(25–35)$ . All peptides studied here have acetylated N-termini and amidated C-termini. The hydrophobic hexapeptide fragments are color coded in red.

## MATERIALS AND METHODS

All peptides have blocked termini to minimize the effect of terminal charges. Lyophilized samples of Ac-Tau(273–284)-NH<sub>2</sub> were purchased from Genscript (Piscataway, NJ, USA). Ac- $\text{A}\beta(25–35)$ -NH<sub>2</sub> was synthesized by FMOC (N-(9-fluorenyl)methoxycarbonyl) chemistry. The peptide was purified by reverse-phase high-performance liquid chromatog-

raphy (HPLC) and characterized by mass spectrometry and amino acid analysis to confirm the purity and integrity of the peptide (>95% purity). Working stock solutions (2 mM for the Ac-Tau(273–284)-NH<sub>2</sub> and 500  $\mu\text{M}$  for Ac- $\text{A}\beta(25–35)$ -NH<sub>2</sub>) were prepared by dissolving the lyophilized peptide in filtered deionized water. This stock was divided into several tubes, flash-frozen in liquid nitrogen, and stored at –80 °C until use. The concentration of peptide samples in IM-MS and AFM experiments is 200  $\mu\text{M}$ . Polydisperse heparin of 11 kDa was from Sigma-Aldrich (St. Louis, MO, USA) and stocked at 1 mM concentration in water at room temperature.

**Ion-Mobility Mass Spectrometry.** In IM-MS experiments, stock solutions were diluted in water to a desired concentration, loaded into gold coated nano-electrospray ionization (ESI) capillaries, and electrosprayed on a home-built instrument.<sup>44</sup> Ions were pulled through a 200 cm long, helium filled drift cell under the influence of a weak electrical field and the drag force created from collisions with buffer gas ions. Particular species with specific  $m/z$  can be mass-selected, and their arrival time distributions can be measured at different pressure to drift voltage ratios ( $P/V$ ), allowing the determination of reduced mobility  $K_0$  and experimental collision cross-sections  $\sigma$ .<sup>45</sup>

**Atomic Force Microscopy.** AFM images were collected using an Asylum MFP-3D-SA system (Asylum Research, Santa Barbara, CA, USA). Details about AFM protocol have been described previously.<sup>46</sup> All images were collected at 1 Hz using 512 × 512 scan points. Images were processed using Igor Pro software and were modified by masking fibrils and then applying a first-order flatten to height images (“Magic Mask” in MFP3D software). All height and length measurements of single fibrils and granular aggregates were conducted using Igor Pro, and each reported value is the average of 20 measurements.

**Molecular Dynamics Simulations.** Temperature-based replica exchange molecular dynamics (T-REMD) simulations were performed using the GROMACS 4.6.3 package<sup>47,48</sup> with a combination of the OPLS-AA force field<sup>49–52</sup> and TIP3P water.<sup>53</sup> In these simulations, the initial conformation of Ac- $\text{A}\beta(25–35)$ -NH<sub>2</sub> is a  $\beta$ -hairpin obtained from T-REMD simulations of the same peptide using the same force field (data not shown), and also consistent with a previous simulation of free terminal  $\text{A}\beta(25–35)$  by Larini and Shea.<sup>31</sup> An initial Ac-Tau(273–284)-NH<sub>2</sub> was chosen from the T-REMD simulations described in ref 30. Structures obtained from these simulations were minimized in the gas phase to mimic the dehydration process that occurred when solution-phase structures enter a solvent-free environment. Their collision cross-sections were computed using the trajectory method available from the Mobcal package.<sup>54,55</sup>

## RESULTS AND DISCUSSION

**Tau(273–284) Binds to  $\text{A}\beta(25–35)$  with High Affinity To Form Heterooligomers.** All IM-MS experiments are performed on a home-built IM-MS instrument described previously.<sup>44</sup> The mass spectra of Ac- $\text{A}\beta(25–35)$ -NH<sub>2</sub>, Ac-Tau(273–284)-NH<sub>2</sub>, and a mixture of both at 1:1 ratio are shown in Figure 2. Water is used in place of buffer to slow down aggregation kinetics, as well as minimize the charge screening effect of buffer ions that may affect aggregation.

The mass spectrum of Ac- $\text{A}\beta(25–35)$ -NH<sub>2</sub> (Figure 2A) contains two major peaks at 550  $m/z$  ( $n/z$  1/2) and 1101  $m/z$  ( $n/z$  1/1), where  $n$  is the  $\text{A}\beta(25–35)$  oligomer size and  $z$  is the

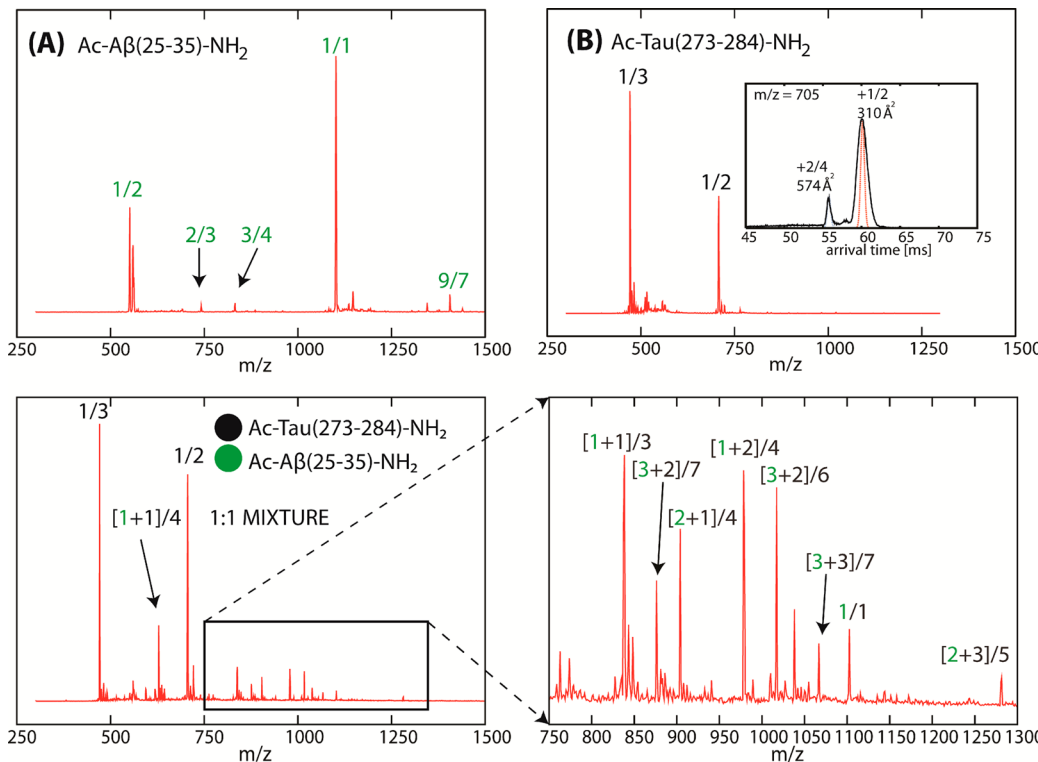


**Figure 2.** ESI–mass spectra of (A) Ac-A $\beta$ (25–35)-NH<sub>2</sub>, (B) Ac-Tau(273–284)-NH<sub>2</sub>, and (C, D) a mixture of the two peptides at 1:1 ratio. The concentration of each peptide is 200  $\mu$ M in water. Each peak is annotated with  $[n + k]/z$  where  $n$  is the oligomer number of Ac-A $\beta$ (25–35)-NH<sub>2</sub>,  $k$  is the oligomer number of Ac-Tau(273–284)-NH<sub>2</sub>, and  $z$  is the net charge of the complex. A representative ATD of the peak at 705  $m/z$  ( $k/z$  1/2) is shown in panel B to illustrate that dimer is the largest Tau oligomer formed under these conditions. Note that the dimer is relatively minor compared to the monomer.

charge. Less intense peaks are observed at 734  $m/z$  ( $n/z$  2/3), 826  $m/z$  ( $n/z$  3/4), and 1407  $m/z$  ( $n/z$  9/7). The arrival time distributions (ATDs) at  $m/z$  other than 1101 contain either a single oligomer species or a single family of conformations (see Supporting Information Figure S1A–C,E). ATDs of the  $n/z$  1/1 peak contain multiple features from dimer to hexamer (Supporting Information Figure S1D). The progression of oligomer cross-sections  $\sigma$  as a function of oligomer size  $n$  (see Figure 3A) shows a positive deviation from the isotropic oligomer model starting at the trimer stage,<sup>56</sup> indicating the formation of extended oligomers. Based on our earlier studies on free terminal A $\beta$ (25–35),<sup>31,32</sup> we can ascribe these extended oligomers to  $\beta$ -rich oligomers. Formation of  $\beta$ -rich oligomers is consistent with the fibril formation propensity of the peptide probed by AFM (see the next section).

The mass spectrum of Ac-Tau(273–284)-NH<sub>2</sub> (Figure 2B) consists of two peaks at 470  $m/z$  ( $k/z$  1/3) and 705  $m/z$  ( $k/z$  1/2) where  $k$  is the oligomer number of Ac-Tau(273–284)-NH<sub>2</sub>. Peaks at higher  $m/z$  are not observed, consistent with the fact that peptide oligomerization occurs at a much slower rate compared to the same peptide in buffer solution.<sup>30</sup> The dimer is the largest oligomer observed (the ATD of the peak at 705  $m/z$  is shown in the inset of Figure 2B). In the absence of aggregation-promoting factors (e.g., heparin), this peptide is unable to form any structural aggregates.<sup>30,39</sup> Furthermore, previous simulations and experimental cross-sections ( $\sigma_{\text{exp}} = 310\text{--}313 \text{ \AA}^2$  for  $z = +2$  and  $+3$ ) suggest that the Tau monomer is in a relatively compact conformation (i.e.,  $\beta$ -turn or  $\beta$ -hairpin). Simulations suggest that aggregation is controlled by a conformational transition of the monomers which later associate to form extended dimers.<sup>30</sup>

The mass spectrum of the mixture (Figure 2C) shows strong peaks for Ac-Tau(273–284)-NH<sub>2</sub> monomer, but the peaks associated with Ac-A $\beta$ (25–35)-NH<sub>2</sub> are strongly suppressed, replaced by several new peaks composed of peptides from both fragments. These mass spectral peaks are annotated with  $[n + k]/z$  where  $n$  is the oligomer number of Ac-A $\beta$ (25–35)-NH<sub>2</sub>,  $k$  is the oligomer number of Ac-Tau(273–284)-NH<sub>2</sub>, and  $z$  is the net charge of the complex. Cross-sections for the mixed aggregate peaks were determined by their ATDs. The experimental cross-sections are accurate to 1%.<sup>44</sup> Figure 3B qualitatively represents the correlated cross-section of Ac-A $\beta$ (25–35)-NH<sub>2</sub> monomer and oligomers extracted from the experimental cross-section of the heterooligomers (see Supporting Information section S2.1 and Table S1),<sup>32</sup> assuming that the Tau conformation is relatively compact (as indicated from simulation<sup>30</sup>). We note that  $\sigma_{\text{corr}}(n)$  can be considered as representative values for the ratios  $\sigma_{\text{exp}}(n,k)/\sigma_{\text{iso}}(n,k)$  between the experimental cross-sections of heterooligomers and the isotropic cross-section model of heterooligomers. Hence if  $\sigma_{\text{exp}}(n,k) \gg \sigma_{\text{iso}}(n,k)$ , we expect a large deviation of  $\sigma_{\text{corr}}(n)$  from the isotropic cross-section of A $\beta$ (25–35) oligomer,  $\sigma_{\text{iso}}(n)$ , indicating that the heterooligomers are nonisotropic.

Under this assumption, we observe that the cross-section deviation occurs as early as heterodimers ( $n = 1, k = 1$ ) and the trend continues for larger oligomers ( $n = 3, k = 2$  and  $n = 2, k = 3$ ). The observation indicates that these heterooligomers adopt extended conformations.<sup>56</sup> This conclusion is generally true regardless of our assumption that the Tau conformation is compact. However, the largest heterooligomers observed in this IM-MS experiment are hexamers, whereas, in the pure Ac-A $\beta$ (25–35)-NH<sub>2</sub> sample, hexamers and nonamers can be

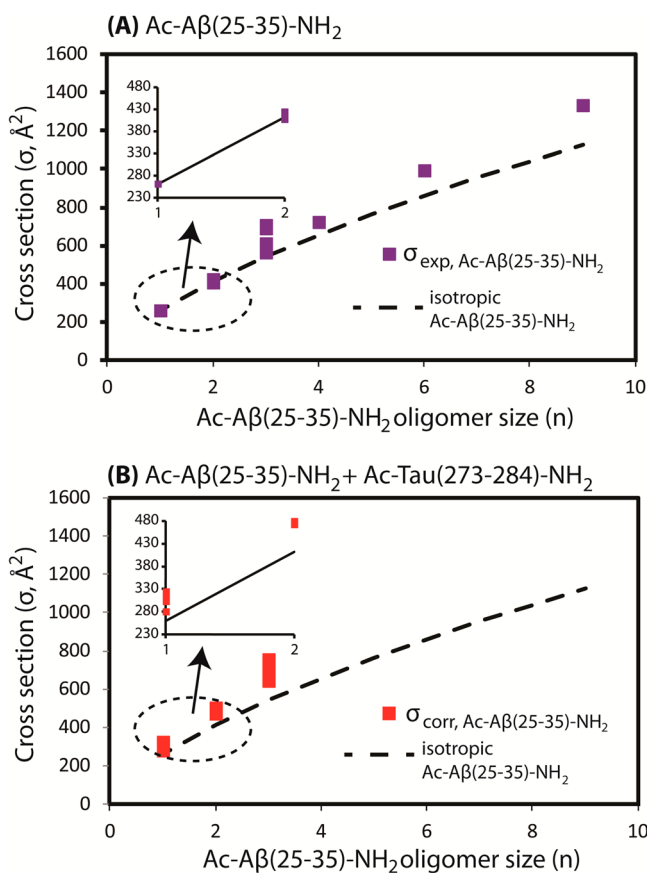


**Figure 3.** (A) Experimental cross-section of Ac- $\text{A}\beta$ (25–35)-NH<sub>2</sub> ( $\sigma_{\text{exp}}$ , Å<sup>2</sup>) as a function of  $n$ . (B) Correlated cross-section of Ac- $\text{A}\beta$ (25–35)-NH<sub>2</sub> + Ac-Tau(273–284)-NH<sub>2</sub> ( $\sigma_{\text{corr}}$ , Å<sup>2</sup>) obtained from the experimental cross-section of heterooligomers. The isotropic cross-sections of Ac- $\text{A}\beta$ (25–35)-NH<sub>2</sub> are shown by the dashed line.

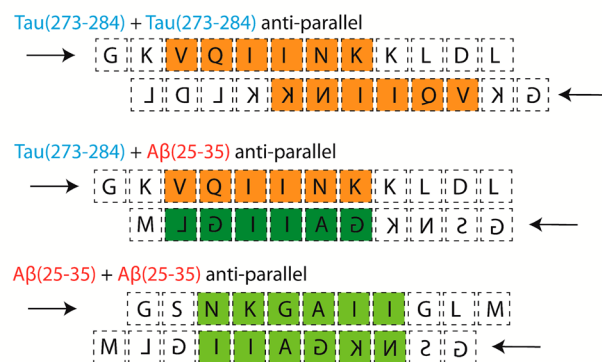
unambiguously detected. Thus, it appears that Ac-Tau(273–284)-NH<sub>2</sub> can trap Ac- $\text{A}\beta$ (25–35)-NH<sub>2</sub> in smaller oligomeric forms.

The significant intensities of the heterodimer peaks (i.e.,  $[1 + 1]/4$  at  $627\text{ m/z}$  and  $[1 + 1]/3$  at  $837\text{ m/z}$ ) indicate that the Tau fragment has a high affinity to bind Ac- $\text{A}\beta(25\text{--}35)\text{-NH}_2$  monomer relative to forming homo-Tau dimers ( $K_d$  in micromolar range; see Supporting Information section S2.2).

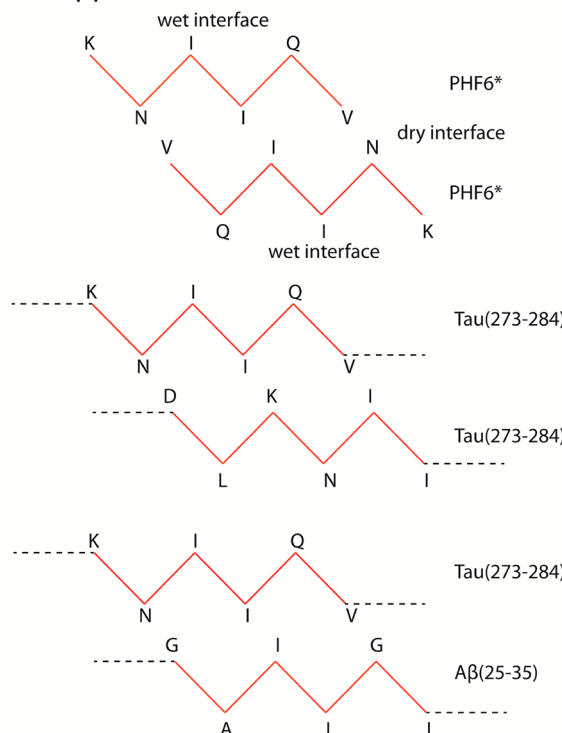
T-REMDS<sup>57</sup> of the heterodimer reveals the existence of at least two major families of structures: compact structures (~40%, in which both Tau and A $\beta$  peptide chains are relatively compact) and extended structures (~10%, where both chains are extended in antiparallel configuration) and other structures in between (see Supporting Information Figure S3).

In terms of cross-sections, two populated clusters of extended antiparallel heterodimers have average cross-sections of  $\sigma_{\text{theory}} = 553$  and  $525 \text{ \AA}^2$  (clusters F and H shown in Supporting Information Figure S3, respectively), which are in good agreement with the  $[1 + 1]/4$  species with the cross-section of  $\sigma_{\text{exp}} = 559 \text{ \AA}^2$ . Similarly, the most populated compact heterodimer clusters have average cross-sections of  $\sigma_{\text{theory}} = 496$  and  $493 \text{ \AA}^2$  (clusters A and B, respectively), which agree well with the  $[1 + 1]/3$  species,  $\sigma_{\text{exp}} = 492 \text{ \AA}^2$ . We note that the theoretical cross-section obtained from the trajectory method available from the Mobcal package,<sup>54,55</sup> from a specific structure, is good to less than 5%.<sup>58,59</sup>

### (A) Single $\beta$ -sheet



### (B) Steric zipper



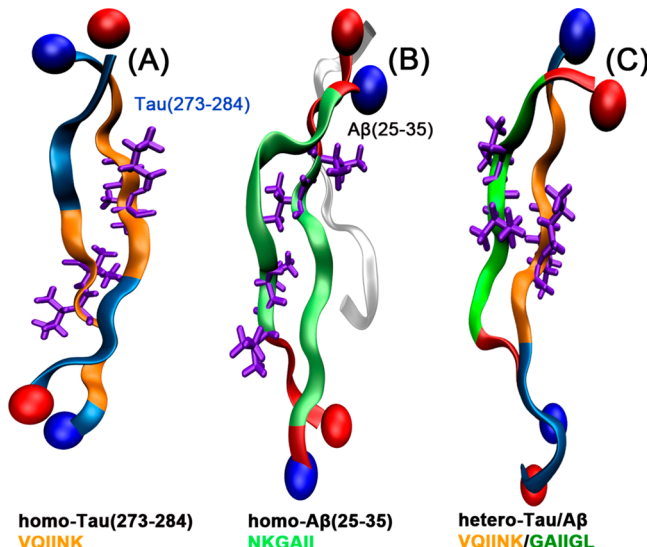
**Figure 4.** Proposed sequence alignments of the peptides in (A) single extended  $\beta$ -sheet and (B) steric zipper conformation.

Figure 4A shows a schematic representation of the alignment of two Tau(273–284) peptides, a mixed Tau(273–284)/A $\beta$ (25–35), and two A $\beta$ (25–35) peptides within a single-layer ideal  $\beta$ -sheet. In the context of a fragment such as Tau(273–284) or full length Tau, the hydrophobic PHF6\* region is blocked between K274 at one end and K280/281 at the other end, making associations between the hydrophobic PHF6\* cores more restricted. In the Ac-Tau(273–284)-NH<sub>2</sub> extended dimer conformation probed in the simulation of Larini et al.,<sup>30</sup> the two PHF6\* segments are shifted away from each other. The extended dimer is stabilized by a weak hydrogen bonding network between backbone atoms of hydrophobic residues such as isoleucine and hydrophilic charged residues such as lysine, consistent with the scheme shown in Figure 4A.

Since the two PHF6\* segments are not within an optimal distance to create a dry interface, the extended dimer structure does not support steric zipper formation optimal for fibrilization.<sup>46</sup> On the other hand, the GAIIGL segment of

Ac- $\text{A}\beta(25\text{--}35)\text{-NH}_2$  can behave similarly to PHF6\*, and the adjacent residues around this segment are less charged than those of Tau. In addition, since Ac- $\text{A}\beta(25\text{--}35)\text{-NH}_2$  is one residue shorter than Ac-Tau(273–284)-NH<sub>2</sub> and the GAIIGL segment is near the C-terminus, Figure 4A also proposes that a better alignment between GAIIGL and PHF6\* can be achieved in antiparallel fashion.

Simulations suggest that both the homodimer of Tau(273–284) and of  $\text{A}\beta(25\text{--}35)$  and the heterodimer of Tau(273–284) and  $\text{A}\beta(25\text{--}35)$  can adopt antiparallel, extended structures with the hydrogen bonding networks shown in Figure 4A. The distributions of distances between hydrophobic cores (between one PHF6\* and another PHF6\* in homo-Tau(273–284) dimer, and between PHF6\* and GAIIGL in the heterodimer) suggest that the hydrophobic cores in the heterodimer can interact more strongly (i.e., within a 5.0 Å distance) than PHF6\* in the homo-Tau(273–284) dimer (see Supporting Information Figure S2 and Figure 5C).



**Figure 5.** Representative structures of the most populated extended clusters obtained from the simulations of (A) blocked terminal homo-Tau(273–284) dimers (see ref 30), (B) free terminal homo- $\text{A}\beta(25\text{--}35)$  trimers (see ref 31) and, (C) blocked terminal hetero-Tau(273–284)/ $\text{A}\beta(25\text{--}35)$  dimers. The interacting hydrophobic cores are highlighted using the same color codes shown in Figure 4. The isoleucine pairs within the hydrophobic stretches are shown in licorice.

According to Figure 4B, the interactions between two  $\beta$ -sheets within a heterodimer steric zipper maintains interactions at the dry interface similar to when PHF6\* is considered alone, with no charged residues in the dry interface. The homo-Tau(273–284) steric zipper, on the other hand, is much less stable, since it has to accommodate charged residues such as lysine and aspartic acid within the dry interface and hydrophobic residues such as isoleucine and leucine at the wet interface. Therefore, it is reasonable to believe that interactions between Ac- $\text{A}\beta(25\text{--}35)\text{-NH}_2$  and Ac-Tau(273–284)-NH<sub>2</sub> can promote  $\beta$ -rich oligomers better than when Ac-Tau(273–284)-NH<sub>2</sub> is incubated separately.

As previously examined from both experiment and theory,<sup>31,32</sup> the aggregation process of  $\text{A}\beta(25\text{--}35)$  involves a structural transition from dimer to trimer stages, in which a compact dimer composed of mainly  $\beta$ -hairpin monomers converts into extended  $\beta$ -rich structures, as shown in Figure 5B.

In these populated  $\beta$ -sheet oligomers (trimer or larger) the hydrophobic cores are NKGAIIL whose locations are more toward the middle of the chains, providing access to steric zipper formation, and eventually fibril formation. NKGAIIL  $\beta$ -sheets can interact in both face-to-face and back-to-back fashions (Protein Data Bank (PDB) ID 3Q2X).<sup>42</sup> Due to the versatility of these interaction motifs, it is likely that these NKGAIIL segments can provide a strong steric zipper interface for  $\text{A}\beta(25\text{--}35)$  to quickly aggregate into fibrils.

The GAIIGL steric zipper (PDB ID 3PZZ) is composed of antiparallel  $\beta$ -sheets interacting face-to-back. This class 6 zipper<sup>43</sup> is often found in weakly aggregating systems such as the islet amyloid polypeptide fragment NFLVHSS (PDB ID 3FTH),<sup>60</sup> and the Enkephalin mutants YVVVF (4OLR) and YVVFL (4ONK).<sup>61</sup> Thus, we can predict that the heterosystem of  $\text{A}\beta(25\text{--}35)$  and Tau(273–284) stabilized by PHF6\*/GAIIGL interactions would self-assemble with slower kinetics into a different aggregate morphology as compared to pure  $\text{A}\beta(25\text{--}35)$ .

**Heteroligomers Composed of  $\text{A}\beta(25\text{--}35)$  Monomer and Oligomers but Not of Tau Oligomers Larger than Dimer.** In Figure 2C, two types of heteroligomers larger than dimers are observed: (1) those with more  $\text{A}\beta$  than Tau peptide chains, which will be referred to as hetero- $\text{A}\beta$  oligomers and (2) those with more Tau than  $\text{A}\beta$ , referred to as hetero-Tau oligomers.

The hetero- $\text{A}\beta$  oligomer peaks (i.e., [2 + 1]/4 at 903 m/z, [3 + 2]/7 at 875 m/z, and [3 + 2]/6 at 1016 m/z) are abundant in intensity indicating that Ac-Tau(273–284)-NH<sub>2</sub> can effectively replace Ac- $\text{A}\beta(25\text{--}35)\text{-NH}_2$  peptide chains to form dimer, trimer, and pentamer, and such processes are favorable. Similar hetero-Tau oligomers are also observed (i.e., [1 + 2]/4 at 979 m/z and [2 + 3]/5 at 1280 m/z). At first glance, the compositions of these hetero-Tau oligomers appear to be similar to those of hetero- $\text{A}\beta$  oligomers, which may suggest that the  $\text{A}\beta$  and Tau peptides can randomly associate to form large oligomers. However, as seen in Figure 6A,C, the ATDs of

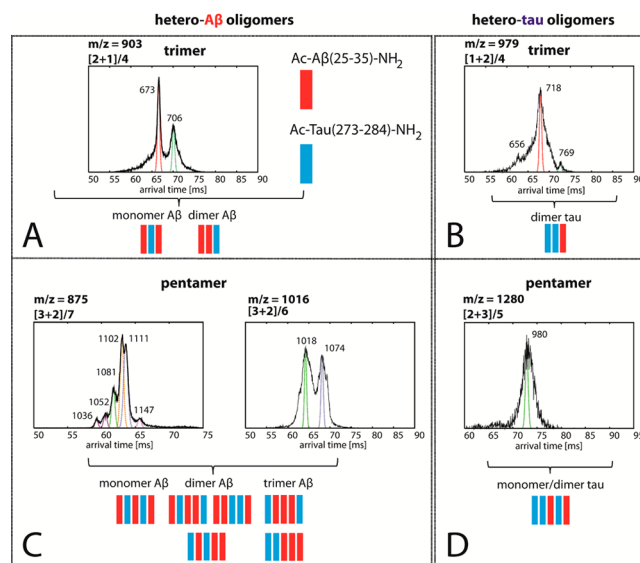


**Figure 6.** Representative ATDs of hetero- $\text{A}\beta$  and hetero-Tau trimer (A,B) and pentamer (C,D) peaks. Each feature is annotated with an experimental cross-section ( $\sigma$ , Å<sup>2</sup>). Possible configurations of the heteroligomers are shown with Ac- $\text{A}\beta(25\text{--}35)\text{-NH}_2$  in red and Ac-Tau(273–284)-NH<sub>2</sub> in blue.

hetero- $\text{A}\beta$  oligomers (i.e., trimer and pentamer) present multiple features and a variety of compact and extended conformations with similar intensities. On the other hand, the ATDs of hetero-Tau oligomers contain a dominant feature with few minor features (Figure 6B,D). A possible explanation is that since homooligomers of Ac-Tau(273–284)-NH<sub>2</sub> larger than dimers are not stable and populated in water, the number of possible arrangements that hetero-Tau oligomers can adopt should always be less than that of hetero- $\text{A}\beta$  oligomers.

The hetero- $\text{A}\beta$  trimer ATD has two peaks with cross-sections of  $\sigma_{\text{exp}} = 673$  and  $706 \text{ \AA}^2$  which mechanistically can be assigned to a trimer composed of two  $\text{A}\beta$  monomers and a Tau monomer intercalating in between (i.e., ABA) and a trimer of an  $\text{A}\beta$  dimer and a Tau monomer (i.e., AAB configuration where A is an Ac- $\text{A}\beta$ (25–35)-NH<sub>2</sub> and B is an Ac-Tau(273–284)-NH<sub>2</sub> monomer). It is worth noting that if both ABA and AAB adopt similar conformations (i.e., extended structures) then the cross-section  $\sigma(\text{AAB})$  should be *larger* than that of  $\sigma(\text{ABA})$ , since the former structure would have more Tau side chains exposed to the outside (Tau is larger in size than  $\text{A}\beta$ ), which increases the collision cross-section. Both features are populated since the  $\text{A}\beta$  monomer and dimer in the sample are abundant (see Supporting Information Figure S1). On the other hand, the hetero-Tau trimer has three features, but the shortest and longest arrival time features are very minor. Statistically the BBA/ABB structures are more likely than the BAB structures (i.e., the BBA/ABB can be formed starting with either AB heterodimer or BB homodimer, whereas the BAB can only be formed from the heterodimer) suggesting this is the structure of the major peak, but this cannot be determined with certainty.

Global stabilization of each quaternary structure often involves not only strong pairwise interactions between adjacent chains but also a network of noncovalent contacts among different subunits. Consequently, the preceding mechanistic description of heterooligomers appears to be too simple. However, the T-REMD simulations of hetero- $\text{A}\beta$  and hetero-Tau trimers qualitatively support such a description. As seen in Figure 7A, the radial distribution function (RDF  $g(r)$ ) computed for the distances between the  $\text{A}\beta$  monomers within the hetero- $\text{A}\beta$  trimers populates several peaks near 0.5 and 1.0 nm. The distance of 0.5 nm indicates that the two Ac- $\text{A}\beta$ (25–35)-NH<sub>2</sub> peptides are adjacent to each other (AAB conformations), whereas that of 1.0 nm suggests the Tau peptide is intercalating in between (ABA conformations). Clustering analysis shows that the conformation of each chain within a structure type can be either compact or extended, which gives rise to a diverse set of conformations. The representative structures and the theoretical cross-sections of the major clusters obtained from the simulation of hetero- $\text{A}\beta$  trimer are shown in Supporting Information Figure S4. While the Tau monomer is relatively extended, the two Ac- $\text{A}\beta$ (25–35)-NH<sub>2</sub> chains can adopt either  $\beta$ -hairpin-like or extended structures. Although the largest experimental cross-section of the hetero- $\text{A}\beta$  trimer is ~10% larger than the reported theoretical cross-sections, if we consider the broad distributions of theoretical cross-sections, the theory and experiment are in good agreement. Some oligomers may be kinetically but not thermodynamically stable. Kinetically stable oligomers have been observed and discussed in our recent study of free terminal  $\text{A}\beta$ (25–35) aggregation.<sup>32</sup>

For the hetero-Tau trimer, all of the dominant peaks of  $g(r)$  are located near 0.5 nm, suggesting that the BBA conformations

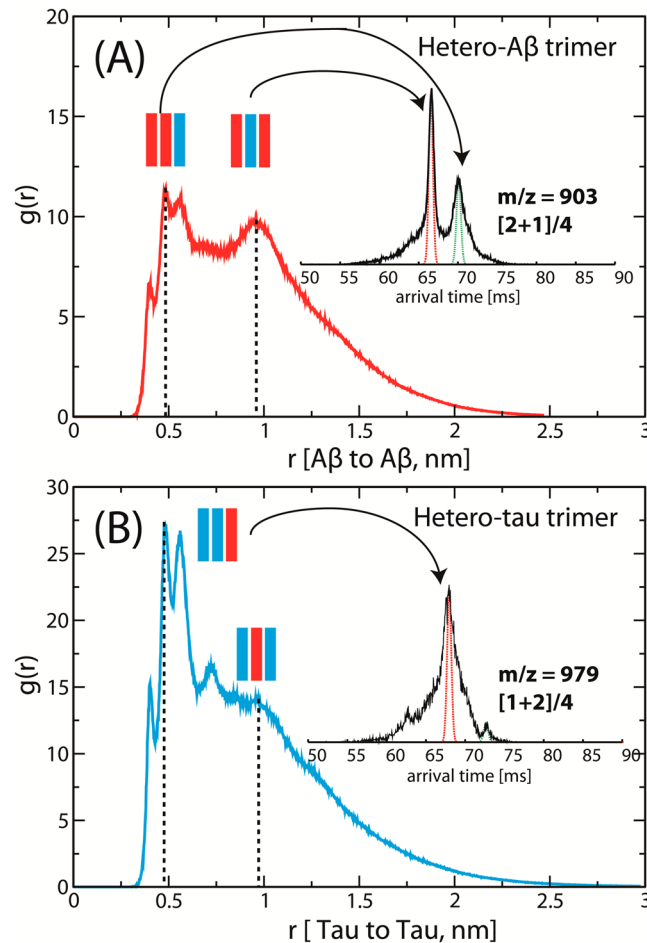


**Figure 7.** Radial distribution functions RDFs  $g(r)$  computed for the distances  $r$  (nm) (A) between the Ac- $\text{A}\beta$ (25–35)-NH<sub>2</sub> monomers within the hetero- $\text{A}\beta$  trimer and (B) between the Ac-Tau(273–284)-NH<sub>2</sub> monomers within the hetero-Tau trimer.

are dominant, in agreement with the assignment made in Figure 6B. Clustering analysis of the hetero-Tau trimers obtained from T-REMD reveals that a majority of extended structures is of BBA type. Some compact, disordered structures are also observed (see Supporting Information Figure S5).

As the size of the heterooligomers grows, a clear distinction between hetero- $\text{A}\beta$  and hetero-Tau oligomers is observed in the IM-MS data. For the heteropentamer, those of  $\text{A}\beta$  contain multiple features in the ATDs corresponding to different species (i.e., there are six possible configurations of hetero- $\text{A}\beta$  pentamer). Since the size of the systems is expensive for high-level MD simulations, we constructed a series of fully extended hetero- $\text{A}\beta$  pentamers corresponding to the configurations shown schematically in Figure 6 (see Supporting Information Figure S6 for the structures obtained from simulation and their theoretical cross-sections). These antiparallel  $\beta$ -sheet models have cross-sections in good agreement with the experiment cross-sections for both charge states ( $z = +6$  and  $+7$ ), suggesting the hetero- $\text{A}\beta$  pentamers adopt extended,  $\beta$ -sheet-like structures.

In contrast, the formation of the single hetero-Tau pentamer is conformationally restricted, as manifested in the ATD containing only one narrow feature. This feature has a smaller cross-section and lower charge state than the hetero- $\text{A}\beta$

pentamers, suggesting that the conformation is relatively more compact.

**Ac-Tau(273–284)-NH<sub>2</sub> Acting as an Inhibitor That Drives Ac-A $\beta$ (25–35)-NH<sub>2</sub> Self-Assembly into Both Granular and Heterofibrillar Aggregates.** Both the IM-MS data and the T-REMD simulations support extended conformations of both Ac-A $\beta$ (25–35)-NH<sub>2</sub> and Ac-Tau(273–284)-NH<sub>2</sub> as early as the heterodimer stage. Figure 8 shows the differences in quantities and morphologies of aggregates in the pure A $\beta$ (25–35), Tau(273–284), and mixture samples. From these data, we conclude that the formation of heteroligomers does not lead to enhanced fibril formation. The behavior of Ac-Tau(273–284)-NH<sub>2</sub> is similar to an inhibitor affecting the aggregation process of Ac-A $\beta$ (25–35)-NH<sub>2</sub>, in which Tau monomer (and some dimer) competitively binds to Ac-A $\beta$ (25–35)-NH<sub>2</sub> monomer and oligomers. For the sample of pure Ac-A $\beta$ (25–35)-NH<sub>2</sub>, abundant fibrillar aggregates are observed (Figure 8A and Supporting Information Figure S7C–F), whereas less fibrils but more granular aggregates are seen in the mixture sample (Figure 8B) and finally no aggregates are found in the pure Tau(273–284) sample (Figure 8C). This raises two questions:

(1) What is the nature of the granular aggregates and fibril-like structures observed in the AFM image of the mixture?

(2) Through which mechanisms does Ac-Tau(273–284)-NH<sub>2</sub> limit the strong aggregation of Ac-A $\beta$ (25–35)-NH<sub>2</sub> and why do the extended conformations of heteroligomers, observed by experiment and by theoretical modeling, not promote abundant formation of fibrils?

To answer the first question, we consider the following possibilities. The granular aggregates can be either (a) homo-Tau aggregates, (b) early globular aggregates of homo-A $\beta$ (25–35), or (c) a type of new aggregate produced by the heteroligomers. Granular aggregates have been observed as intermediates in some Tau fragment aggregation<sup>62</sup> but not specifically for Ac-Tau(273–284)-NH<sub>2</sub> in the absence of aggregation-promoting factor (see Figure 8C). In the presence of 11 kDa polydisperse heparin at 4:1 peptide/heparin ratio, aggregation of Ac-Tau(273–284)-NH<sub>2</sub> in water occurs within 1 h to form abundant well-defined aggregates (see Supporting Information Figure S7A,B) and no granular aggregates are detected. Thus, the granular aggregates observed in the mixture sample should not be from the Tau itself; this eliminates option a of homo-Tau oligomers.

We now consider option b: homo-A $\beta$  oligomers. We note that, in our experiment, fresh Ac-A $\beta$ (25–35)-NH<sub>2</sub> forms large,  $\beta$ -rich oligomers within a short time after sample preparation and forms fibrillar aggregates within an hour (Supporting Information Figure S7C,D), suggesting that there is not a noticeable morphology transition occurring during the aggregation of Ac-A $\beta$ (25–35)-NH<sub>2</sub>. A few small aggregates are sparsely distributed at the edges of the AFM slide (Supporting Information Figure S7G,H). However, these aggregates vary widely in length and have on average a lower height than the granular aggregates observed in the mixture sample which suggests a different composition (see Table 1). We consider the possibility that Ac-Tau(273–284)-NH<sub>2</sub> acts as an inhibitor to efficiently disassemble Ac-A $\beta$ (25–35)-NH<sub>2</sub> fibrils into globular aggregates. In other words, the interactions between Ac-Tau(273–284)-NH<sub>2</sub> and Ac-A $\beta$ (25–35)-NH<sub>2</sub> must be significantly stronger than A $\beta$ (25–35) with itself in order to successfully compete with existing interactions between A $\beta$  chains inside the fibrils. To examine whether Ac-

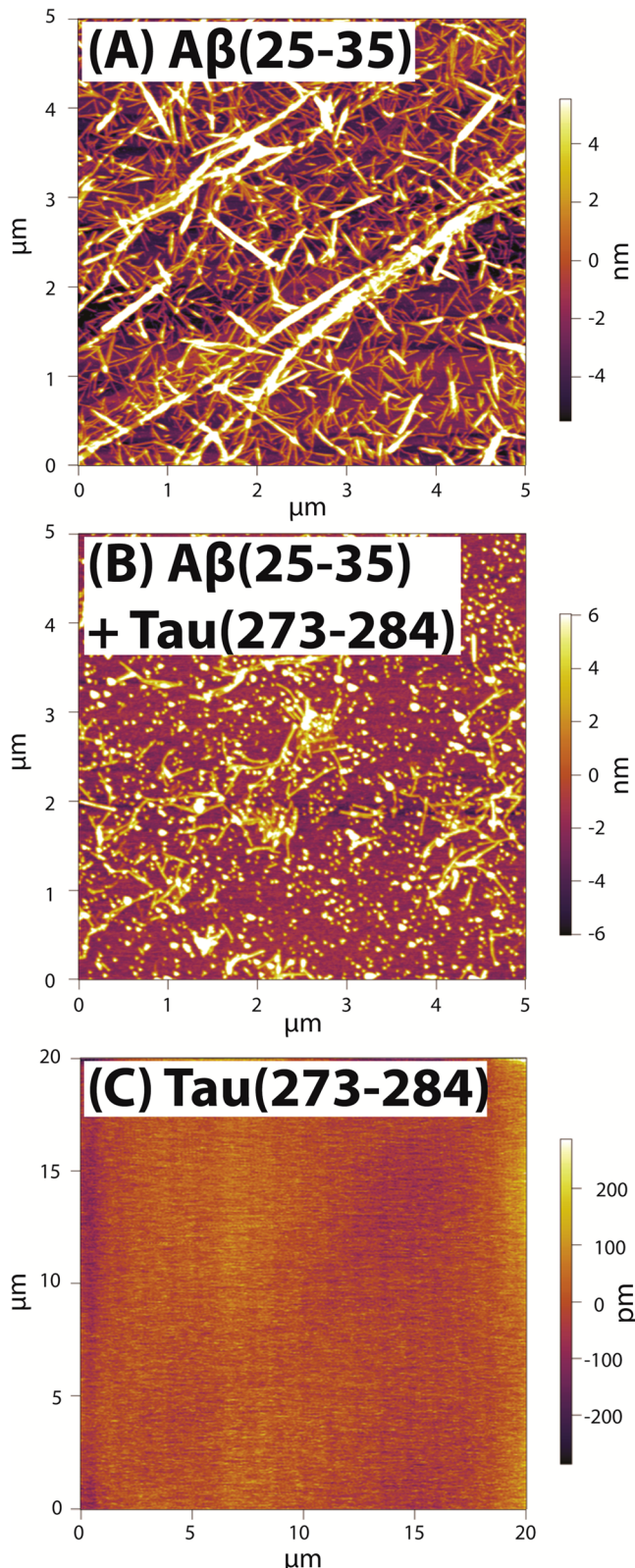


**Figure 8.** Representative AFM images of (A, B) 1 week incubated 200  $\mu\text{M}$  Ac- $\beta$ (25–35)-NH<sub>2</sub> in water without Ac-Tau(273–284)-NH<sub>2</sub> and with Ac-Tau(273–284)-NH<sub>2</sub> at the ratio of 1:1 and (C) 2 week incubated 200  $\mu\text{M}$  Ac-Tau(273–284)-NH<sub>2</sub> in water.

Tau(273–284)-NH<sub>2</sub> can disaggregate Ac- $\beta$ (25–35)-NH<sub>2</sub> fibrils, fresh Tau was added to a week-old sample containing extensive fibrillar aggregates of Ac- $\beta$ (25–35)-NH<sub>2</sub>. No

**Table 1. Dimension (Height (nm) and Length (nm)) of the Aggregates Observed by AFM for the Samples of Pure Ac- $\text{A}\beta(25\text{--}35)\text{-NH}_2$  and 1:1 Mixture of Ac- $\text{A}\beta(25\text{--}35)\text{-NH}_2$  and Ac-Tau(273–284)-NH<sub>2</sub> at 200  $\mu\text{M}$**

type of aggregate	figure	height (nm)	length (nm)
$\text{A}\beta(25\text{--}35)$ fibrils	8A	4.18 $\pm$ 0.36	332.7 $\pm$ 29.9
$\text{A}\beta(25\text{--}35)$ small aggregates	S7H,I <sup>a</sup>	5.16 $\pm$ 0.61	n/a
mixed fibrils	8B	5.20 $\pm$ 0.26	443.8 $\pm$ 22.4
granular aggregates	8B	6.50 $\pm$ 0.51	81.7 $\pm$ 5.4

<sup>a</sup>Supporting Information.

decrease in fibrillar aggregate abundance was observed. From the data, it is clear that Ac-Tau(273–284)-NH<sub>2</sub> does not disassemble Ac- $\text{A}\beta(25\text{--}35)\text{-NH}_2$  aggregates, which eliminates b as an option (see Supporting Information Figure S8).

Finally, we turn to option c, the possibility of forming mixed aggregates. As seen in IM-MS and in simulations, Ac-Tau(273–284)-NH<sub>2</sub> and Ac- $\text{A}\beta(25\text{--}35)\text{-NH}_2$  can interact. It is hence reasonable to assume that Ac-Tau(273–284)-NH<sub>2</sub> can decorate existing Ac- $\text{A}\beta(25\text{--}35)\text{-NH}_2$  oligomers and proto-fibrils by occasionally adding on the growing aggregate in place of new  $\text{A}\beta$  chains. The more  $\text{A}\beta$  that are replaced by Tau, the less prone the oligomers are to grow further since there are structural differences between hetero- $\text{A}\beta$  and hetero-Tau oligomers. Therefore, option c is the most probable. Compact hetero-Tau and some hetero- $\text{A}\beta$  oligomers can trap Ac- $\text{A}\beta(25\text{--}35)\text{-NH}_2$  oligomers in  $\beta$ -hairpin or  $\beta$ -turn conformations, leading to the formation of granular aggregates. Since Ac-Tau(273–284)-NH<sub>2</sub> monomer is larger than Ac- $\text{A}\beta(25\text{--}35)\text{-NH}_2$  monomer in size, the fibrils grown from heterooligomers would be more likely to have larger dimensions than the pure Ac- $\text{A}\beta(25\text{--}35)\text{-NH}_2$  fibrils. Additional AFM measurements show that both heights and lengths of the fibrils and granular features formed in the mixture sample are greater than those of the pure Ac- $\text{A}\beta(25\text{--}35)\text{-NH}_2$  (see Table 1). In these measurements, only the dimension of individual fibrils is taken into account, and the larger features which are probably clusters of several fibrils are not considered.

For the second question, we first consider the mechanisms through which  $\text{A}\beta(25\text{--}35)$  can aggregate. The simulations of Ac- $\text{A}\beta(25\text{--}35)\text{-NH}_2$  by Wei et al.<sup>28</sup> show the existence of a V-shaped parallel dimer, an out of register antiparallel dimer, and an intertwined  $\beta$ -hairpin conformation at small populations as potential seeds for amyloid formation. The major driving force for the first two families of structures is hydrophobic interactions between GAIIGL segments. Larini and Shea,<sup>31</sup> in simulations of  $\text{A}\beta(25\text{--}35)$ , suggest that the transition from  $\beta$ -hairpin  $\text{A}\beta(25\text{--}35)$  monomer to extended structures of oligomers is regulated by a competition between electrostatics and hydrophobic effects. Electrostatics dominate for dimer formation to produce mainly compact structures composed of two tilted  $\beta$ -hairpin monomers, whereas hydrophobic interactions facilitate the  $\beta$ -sheet trimers and tetramers. They also propose the role of  $\beta$ -hairpin structure in a kinetic growth model as a means to stabilize flat  $\beta$ -sheets and prevent newly formed oligomers from hydrophobic collapse. When Ac-Tau(273–284)-NH<sub>2</sub> and Ac- $\text{A}\beta(25\text{--}35)\text{-NH}_2$  form extended dimers, or Ac-Tau(273–284)-NH<sub>2</sub> intercalates between Ac- $\text{A}\beta(25\text{--}35)\text{-NH}_2$  hairpins at the trimer or pentamer, Tau limits the influences of  $\beta$ -hairpin structure in the growth of  $\text{A}\beta(25\text{--}35)$  fibrils and subsequently decreases the aggregation propensity. By replacing the hydrophobic core of NKGAI

NKGAI with PHF6\*/GAIIGL, and limiting the role of  $\text{A}\beta(25\text{--}35)$  hairpins, Ac-Tau(273–284)-NH<sub>2</sub> decreases the aggregation propensity of Ac- $\text{A}\beta(25\text{--}35)\text{-NH}_2$ . The hetero- $\text{A}\beta$  oligomers are relatively extended, but not as aggregation-prone as the homo- $\text{A}\beta$  oligomers, due to the mismatches in side-chain interdigitations and their heterogeneity. The presence of a few Tau chains within the heterocomplexes may decrease the ability to self-associate, but the system is still able to grow further into fibrils, which is consistent with what has been observed in the AFM image of the mixture (Figure 8B).

It has been long predicted that heterotypic  $\beta$ -sheet and steric zipper structures can exist. Eisenberg and co-workers have shown that the macroscopic morphologies and abundances of fibrillar aggregates formed in binary mixtures of different  $\text{A}\beta$  segments are distinct from the component segments.<sup>42</sup> However, no X-ray crystal structures of heterotypic  $\beta$ -sheet and steric zipper have been solved. One of the possible explanations is that even in a binary system of two short peptides, the tendency of homotypic structure formation is dominant, and crystallization is highly dependent upon the kinetics and growth conditions which are very selective. The two factors often promote the crystallization of one type or the other, but not heterotypic crystals. Thus, IM-MS appears to be a versatile technique to approach this problem. Previous work has shown that the experimental cross-sections of aggregating peptide oligomers are in good agreement with X-ray crystal structures.<sup>56</sup> Furthermore, even a small amount of heterooligomers can be detected with this technique.

## SUMMARY AND CONCLUSIONS

(1) Using a combination of experimental and theoretical techniques, we are able to identify the interactions promoting and stabilizing Ac- $\text{A}\beta(25\text{--}35)\text{-NH}_2$ /Ac-Tau(273–284)-NH<sub>2</sub> heterooligomers. The formation of heterooligomers triggers conformation transitions from compact to extended forms for both peptides as early as the dimer stage. Ac-Tau(273–284)-NH<sub>2</sub> monomer prefers to associate with an Ac- $\text{A}\beta(25\text{--}35)\text{-NH}_2$  monomer over another Tau monomer as shown by the populations of heterodimer and homo-Tau dimer in the mixture. The intercalation of Ac-Tau(273–284)-NH<sub>2</sub> monomers between Ac- $\text{A}\beta(25\text{--}35)\text{-NH}_2$  monomers (and oligomers) is a probable mechanism allowing large heterooligomers to grow with a wide range of configurations and conformations.

(2) The heterogeneity of the heterooligomers and mismatches in side-chain interdigitations limit (but do not fully eliminate) aggregation. The hetero-Tau oligomers can be trapped at relatively small sizes, producing granular aggregates. On the other hand, the architectures of hetero- $\text{A}\beta$  oligomers contain  $\beta$ -rich content, which later can grow into heterofibrils, as illustrated in Figure 9.

(3) A possible source of toxicity of early  $\text{A}\beta$  oligomers may lie in their ability to bind Tau monomers, thereby decreasing the population of Tau needed to regulate microtubule dynamics. Other possible pathways to toxicity lie in the structures of the heterooligomers formed by the interactions of different Tau to  $\text{A}\beta$  fragments, which awaits a further systematic investigation.

(4) IM-MS can probe conformations and abundances of heterooligomers, demonstrating its capacity as a promising screening method to identify important segments from different aggregating proteins (e.g.,  $\text{A}\beta$ , Tau, prion, islet amyloid polypeptide) that can interact with each other to form heterotypic structures. These studies will provide insights into

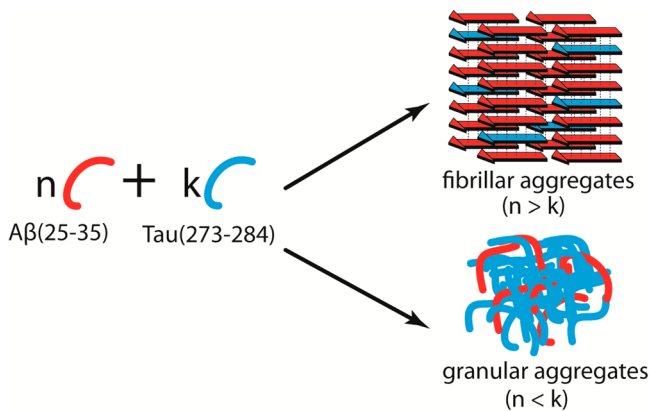


**Figure 9.** Illustration of how fibrillar and granular aggregates can be formed in the mixture of Ac- $\text{A}\beta(25\text{--}35)\text{-NH}_2$  and Ac-Tau(273–284)- $\text{NH}_2$ . The morphologies of the aggregates are determined by the population of the individual peptides.

synergy effects of protein markers responsible for aggregation-related diseases, which are currently challenging to unravel.

## ■ ASSOCIATED CONTENT

### S Supporting Information

Text giving full descriptions of experimental and theoretical protocols and accompanying references, additional figures from the analysis of T-REMD simulation data, additional AFM images, and ATDs of pure Ac- $\text{A}\beta(25\text{--}35)\text{-NH}_2$  and pure Ac-Tau(273–284)- $\text{NH}_2$ , and a table listing collision cross-sections for oligomers of  $\text{A}\beta(25\text{--}35)$ . This material is available free of charge via the Internet at <http://pubs.acs.org>.

## ■ AUTHOR INFORMATION

### Corresponding Author

\*E-mail: [bowers@chem.ucsb.edu](mailto:bowers@chem.ucsb.edu). Tel.: +1-805-893-2673.

### Notes

The authors declare no competing financial interest.

## ■ ACKNOWLEDGMENTS

We thank Ms. Margaret Condron and Prof. David B. Teplow for supplying the Ac- $\text{A}\beta(25\text{--}35)\text{-NH}_2$  peptide. T.D.D. thanks Dr. Nichole E. LaPointe and Ms. Kaitlin McDermott for useful discussion. We gratefully acknowledge support from the National Science Foundation Grant CHE-1301032 (M.T.B.) for personnel support, and the National Institutes of Health Grant 1R01AG047116-01 (M.T.B.) for material support and partial personal support. N.J.E. acknowledges the National Science Foundation Graduate Student Research Fellowship. S.K.B. acknowledges funding from the MURI and DURIP programs of the U.S. Army Research Laboratory and U.S. Army Research Office under Grant Nos. DAAD 19-03-1-0121 and W911NF-09-1-0280 for purchase of the AFM instrument. We acknowledge the Texas Advanced Computing Center (TACC) at the University of Texas at Austin for providing HPC resources through the XSEDE Grant No. TG-MCA05S027 (J.-E.S.) and also support from the Center for Scientific Computing at the CNSI and MRL: NSF MRSEC (Grant DMR-1121053) and NSF Grant CNS-0960316.

## ■ REFERENCES

- (1) Buee, L.; Bussiere, T.; Buee-Scherrer, V.; Delacourte, A.; Hof, P. R. Tau Protein Isoforms, Phosphorylation and Role in Neurodegenerative Disorders. *Brain Res. Rev.* **2000**, *33*, 95–130.
- (2) Binder, L. I.; Guillozet-Bongaarts, A. L.; Garcia-Sierra, F.; Berry, R. W. Tau, Tangles, and Alzheimer's Disease. *Biochim. Biophys. Acta* **2005**, *1739*, 216–223.
- (3) Wolfe, M. S. Tau Mutations in Neurodegenerative Diseases. *J. Biol. Chem.* **2009**, *284*, 6021–6025.
- (4) Goedert, M.; Spillantini, M. G. Tau Mutations in Frontotemporal Dementia Ftdp-17 and Their Relevance for Alzheimer's Disease. *Biochim. Biophys. Acta* **2000**, *1502*, 110–121.
- (5) Hardy, J.; Selkoe, D. J. The Amyloid Hypothesis of Alzheimer's Disease: Progress and Problems on the Road to Therapeutics. *Science* **2002**, *297*, 353–356.
- (6) Bernstein, S. L.; Dupuis, N. F.; Lazo, N. D.; Wyttenbach, T.; Condron, M. M.; Bitan, G.; Teplow, D. B.; Shea, J.-E.; Ruotolo, B. T.; Robinson, C. V.; Bowers, M. T. Amyloid- $\beta$  Protein Oligomerization and the Importance of Tetramers and Dodecamers in the Aetiology of Alzheimer's Disease. *Nat. Chem.* **2009**, *1*, 326–331.
- (7) Laganowsky, A.; Liu, C.; Sawaya, M. R.; Whitelegge, J. P.; Park, J.; Zhao, M. L.; Pensalfini, A.; Soriaga, A. B.; Landau, M.; Teng, P. K.; Cascio, D.; Glabe, C.; Eisenberg, D. Atomic View of a Toxic Amyloid Small Oligomer. *Science* **2012**, *335*, 1228–1231.
- (8) Gotz, J.; Chen, F.; van Dorpe, J.; Nitsch, R. M. Formation of Neurofibrillary Tangles in P301L Tau Transgenic Mice Induced by  $\text{A}\beta$  42 Fibrils. *Science* **2001**, *293*, 1491–1495.
- (9) Lee, H. G.; Zhu, X. W.; Castellani, R. J.; Nunomura, A.; Perry, G.; Smith, M. A. Amyloid- $\beta$  in Alzheimer Disease: The Null Versus the Alternate Hypotheses. *J. Pharmacol. Exp. Ther.* **2007**, *321*, 823–829.
- (10) Giannakopoulos, P.; Herrmann, F. R.; Bussiere, T.; Bouras, C.; Kovari, E.; Perl, D. P.; Morrison, J. H.; Gold, G.; Hof, P. R. Tangle and Neuron Numbers, but Not Amyloid Load, Predict Cognitive Status in Alzheimer's Disease. *Neurology* **2003**, *60*, 1495–1500.
- (11) Williams, T. L.; Serpell, L. C. Membrane and Surface Interactions of Alzheimer's  $\text{A}\beta$  Peptide—Insights into the Mechanism of Cytotoxicity. *FEBS J.* **2011**, *278*, 3905–3917.
- (12) Bokvist, M.; Lindstrom, F.; Watts, A.; Grobner, G. Two Types of Alzheimer's  $\beta$ -Amyloid (1–40) Peptide Membrane Interactions: Aggregation Preventing Transmembrane Anchoring Versus Accelerated Surface Fibril Formation. *J. Mol. Biol.* **2004**, *335*, 1039–1049.
- (13) LaFerla, F. M.; Green, K. N.; Oddo, S. Intracellular Amyloid- $\beta$  in Alzheimer's Disease. *Nat. Rev. Neurosci.* **2007**, *8*, 499–509.
- (14) Olzscha, H.; Schermann, S. M.; Woerner, A. C.; Pinkert, S.; Hecht, M. H.; Tartaglia, G. G.; Vendruscolo, M.; Hayer-Hartl, M.; Hartl, F. U.; Vabulas, R. M. Amyloid-Like Aggregates Sequester Numerous Metastable Proteins with Essential Cellular Functions. *Cell* **2011**, *144*, 67–78.
- (15) King, M. E.; Kan, H. M.; Baas, P. W.; Erisir, A.; Glabe, C. G.; Bloom, G. S. Tau-Dependent Microtubule Disassembly Initiated by Prefibrillar  $\beta$ -Amyloid. *J. Cell Biol.* **2006**, *175*, 541–546.
- (16) Lewis, J.; Dickson, D. W.; Lin, W. L.; Chisholm, L.; Corral, A.; Jones, G.; Yen, S. H.; Sahara, N.; Skipper, L.; Yager, D.; Eckman, C.; Hardy, J.; Hutton, M.; McGowan, E. Enhanced Neurofibrillary Degeneration in Transgenic Mice Expressing Mutant Tau and APP. *Science* **2001**, *293*, 1487–1491.
- (17) Jin, M.; Shepardson, N.; Yang, T.; Chen, G.; Walsh, D.; Selkoe, D. J. Soluble Amyloid  $\beta$ -Protein Dimers Isolated from Alzheimer Cortex Directly Induce Tau Hyperphosphorylation and Neuritic Degeneration. *Proc. Natl. Acad. Sci. U. S. A.* **2011**, *108*, 5819–5824.
- (18) Zempel, H.; Luedtke, J.; Kumar, Y.; Biernat, J.; Dawson, H.; Mandelkow, E.; Mandelkow, E. M. Amyloid- $\beta$  Oligomers Induce Synaptic Damage Via Tau-Dependent Microtubule Severing by TTLL6 and Spastin. *EMBO J.* **2013**, *32*, 2920–2937.
- (19) Zheng, W. H.; Bastianetto, S.; Mennicken, F.; Ma, W.; Kar, S. Amyloid- $\beta$  Peptide Induces Tau Phosphorylation and Loss of Cholinergic Neurons in Rat Primary Septal Cultures. *Neuroscience* **2002**, *115*, 201–211.

- (20) Ma, Q. L.; Yang, F.; Rosario, E. R.; Ubeda, O. J.; Beech, W.; Gant, D. J.; Chen, P. P.; Hudspeth, B.; Chen, C.; Zhao, Y.; Vinters, H. V.; Frautschy, S. A.; Cole, G. M.  $\beta$ -Amyloid Oligomers Induce Phosphorylation of Tau and Inactivation of Insulin Receptor Substrate Via C-Jun N-Terminal Kinase Signaling: Suppression by Omega-3 Fatty Acids and Curcumin. *J. Neurosci.* **2009**, *29*, 9078–9089.
- (21) Tokutake, T.; Kasuga, K.; Yajima, R.; Sekine, Y.; Tezuka, T.; Nishizawa, M.; Ikeuchi, T. Hyperphosphorylation of Tau Induced by Naturally Secreted Amyloid-B at Nanomolar Concentrations Is Modulated by Insulin-Dependent AKT-GSK3 $\beta$  Signaling Pathway. *J. Biol. Chem.* **2012**, *287*, 35222–35233.
- (22) Ittner, L. M.; Gotz, J. Amyloid-Beta and Tau—A Toxic Pas De Deux in Alzheimer's Disease. *Nat. Rev. Neurosci.* **2011**, *12*, 65–72.
- (23) Guo, J.-P.; Arai, T.; Miklossy, J.; McGeer, P. L.  $A\beta$  and Tau Form Soluble Complexes That May Promote Self Aggregation of Both into the Insoluble Forms Observed in Alzheimer's Disease. *Proc. Natl. Acad. Sci. U. S. A.* **2006**, *103*, 1953–1958.
- (24) Rapoport, M.; Dawson, H. N.; Binder, L. I.; Vitek, M. P.; Ferreira, A. Tau Is Essential to  $\beta$ -Amyloid-Induced Neurotoxicity. *Proc. Natl. Acad. Sci. U. S. A.* **2002**, *99*, 6364–6369.
- (25) Busciglio, J.; Lorenzo, A.; Yeh, J.; Yankner, B. A.  $\beta$ -Amyloid Fibrils Induce Tau-Phosphorylation and Loss of Microtubule-Binding. *Neuron* **1995**, *14*, 879–888.
- (26) Ferreira, A.; Lu, Q.; Orecchio, L.; Kosik, K. S. Selective Phosphorylation of Adult Tau Isoforms in Mature Hippocampal Neurons Exposed to Fibrillar  $A\beta$ . *Mol. Cell. Neurosci.* **1997**, *9*, 220–234.
- (27) Takashima, A.; Honda, T.; Yasutake, K.; Michel, G.; Murayama, O.; Murayama, M.; Ishiguro, K.; Yamaguchi, H. Activation of Tau Protein Kinase I/Glycogen Synthase Kinase-3beta by Amyloid- $\beta$  Peptide (25–35) Enhances Phosphorylation of Tau in Hippocampal Neurons. *Neurosci. Res.* **1998**, *31*, 317–323.
- (28) Wei, G.; Jewett, A. I.; Shea, J. E. Structural Diversity of Dimers of the Alzheimer Amyloid- $\beta$ (25–35) Peptide and Polymorphism of the Resulting Fibrils. *Phys. Chem. Chem. Phys.* **2010**, *12*, 3622–3629.
- (29) Wei, G. H.; Shea, J. E. Effects of Solvent on the Structure of the Alzheimer Amyloid- $\beta$  (25–35) Peptide. *Biophys. J.* **2006**, *91*, 1638–1647.
- (30) Larini, L.; Gessel, M. M.; Lapointe, N. E.; Do, T. D.; Bowers, M. T.; Feinstein, S. C.; Shea, J. E. Initiation of Assembly of Tau(273–284) and Its  $\Delta$ K280 Mutant: An Experimental and Computational Study. *Phys. Chem. Chem. Phys.* **2013**, *15*, 8916–8928.
- (31) Larini, L.; Shea, J. E. Role of B-Hairpin Formation in Aggregation: The Self-Assembly of the Amyloid- $\beta$  (25–35) Peptide. *Biophys. J.* **2012**, *103*, 576–586.
- (32) Bleiholder, C.; Do, T. D.; Wu, C.; Economou, N. J.; Bernstein, S. S.; Buratto, S. K.; Shea, J.-E.; Bowers, M. T. Ion Mobility Spectrometry Reveals the Mechanism of Amyloid Formation of  $A\beta$ (25–35) and Its Modulation by Inhibitors at the Molecular Level: Epigallocatechin Gallate and Scyllo-Inositol. *J. Am. Chem. Soc.* **2013**, *135*, 16926–16937.
- (33) Kittner, M.; Knecht, V. Disordered Versus Fibril-Like Amyloid- $\beta$  (25–35) Dimers in Water: Structure and Thermodynamics. *J. Phys. Chem. B* **2010**, *114*, 15288–15295.
- (34) Clementi, M. E.; Marini, S.; Coletta, M.; Orsini, F.; Giardina, B.; Misiti, F.  $A\beta$ (31–35) and  $A\beta$ (25–35) Fragments of Amyloid Beta-Protein Induce Cellular Death through Apoptotic Signals: Role of the Redox State of Methionine-35. *FEBS Lett.* **2005**, *579*, 2913–2918.
- (35) Pike, C. J.; Walencewiczawasserman, A. J.; Kosmoski, J.; Cribbs, D. H.; Glabe, C. G.; Cotman, C. W. Structure-Activity Analyses of  $\beta$ -Amyloid Peptides - Contributions of the Beta-25–35 Region to Aggregation and Neurotoxicity. *J. Neurochem.* **1995**, *64*, 253–265.
- (36) Moore, C. L.; Huang, M. H.; Robbennolt, S. A.; Voss, K. R.; Combs, B.; Gamblin, T. C.; Goux, W. J. Secondary Nucleating Sequences Affect Kinetics and Thermodynamics of Tau Aggregation. *Biochemistry* **2011**, *50*, 10876–10886.
- (37) Li, W. K.; Lee, V. M. Y. Characterization of Two VQIXXX Motifs for Tau Fibrillization in Vitro. *Biochemistry* **2006**, *45*, 15692–15701.
- (38) Goux, W. J.; Kopplin, L.; Nguyen, A. D.; Leak, K.; Rutkofsky, M.; Shanmuganandam, V. D.; Sharma, D.; Inouye, H.; Kirschner, D. A. The Formation of Straight and Twisted Filaments from Short Tau Peptides. *J. Biol. Chem.* **2004**, *279*, 26868–26875.
- (39) von Bergen, M.; Barghorn, S.; Li, L.; Marx, A.; Biernat, J.; Mandelkow, E. M.; Mandelkow, E. Mutations of Tau Protein in Frontotemporal Dementia Promote Aggregation of Paired Helical Filaments by Enhancing Local  $\beta$ -Structure. *J. Biol. Chem.* **2001**, *276*, 48165–48174.
- (40) Miller, Y.; Ma, B.; Nussinov, R. Synergistic Interactions between Repeats in Tau Protein and  $A\beta$  Amyloids May Be Responsible for Accelerated Aggregation Via Polymorphic States. *Biochemistry* **2011**, *50*, 5172–5181.
- (41) Levy, S. F.; Leboeuf, A. C.; Massie, M. R.; Jordan, M. A.; Wilson, L.; Feinstein, S. C. Three- and Four-Repeat Tau Regulate the Dynamic Instability of Two Distinct Microtubule Subpopulations in Qualitatively Different Manners. Implications for Neurodegeneration. *J. Biol. Chem.* **2005**, *280*, 13520–13528.
- (42) Colletiera, J.-P.; Laganowsky, A.; Landau, M.; Zhao, M.; Soriaga, A. B.; Goldschmidt, L.; Flot, D.; Cascio, D.; Sawaya, M. R.; Eisenberg, D. Molecular Basis for Amyloid- $\beta$  Polymorphism. *Proc. Natl. Acad. Sci. U. S. A.* **2011**, *108*, 16938–16943.
- (43) Sawaya, M. R.; Sambashivan, S.; Nelson, R.; Ivanova, M. I.; Sievers, S. A.; Apostol, M. I.; Thompson, M. J.; Balbirnie, M.; Wiltzius, J. J. W.; MacFarlane, H. T.; Madsen, A. Ø.; Riek, C.; Eisenberg, D. Atomic Structures of Amyloid Cross- $\beta$  Spines Reveal Varied Steric Zippers. *Nature* **2007**, *447*, 453–457.
- (44) Kemper, P. R.; Dupuis, N. F.; Bowers, M. T. A New, Higher Resolution, Ion Mobility Mass Spectrometer. *Int. J. Mass. Spectrom.* **2009**, *287*, 46–57.
- (45) Mason, E. A. *Transport Properties of Ions in Gases*, 99th ed.; John Wiley & Sons: New York, 1988.
- (46) Do, T. D.; Economou, N. J.; LaPointe, N. E.; Kincannon, W. M.; Bleiholder, C.; Feinstein, S. C.; Teplow, D. B.; Buratto, S. K.; Bowers, M. T. Factors That Drive Peptide Assembly and Fibril Formation: Experimental and Theoretical Analysis of Sup35 NNQQNY Mutants. *J. Phys. Chem. B* **2013**, *117*, 8436–8446.
- (47) Hess, B.; Kutzner, C.; van der Spoel, D.; Lindahl, E. Gromacs 4: Algorithms for Highly Efficient, Load-Balanced, and Scalable Molecular Simulation. *J. Chem. Theory Comput.* **2008**, *4*, 435–437.
- (48) Spoel, D. V. D.; Lindahl, E.; Hess, B.; Groenhof, G.; Mark, A. E.; Berendsen, H. J. C. Gromacs: Fast, Flexible, and Free. *J. Comput. Chem.* **2005**, *26*, 1701–1718.
- (49) Damm, W.; Halgren, T. A.; Murphy, R. B.; Smolyrev, A. M.; Friesner, R. A.; Jorgensen, W. L. OPLS\_2002: A New Version of the OPLS-AA Force Field. *Abstr. Pap. Am. Chem. Soc.* **2002**, *224*, U471–U471.
- (50) Halgren, T. A.; Murphy, R. B.; Jorgensen, W. L.; Friesner, R. A. Extending the OPLS-AA Force Field for Ligand Functionality. *Abstr. Pap. Am. Chem. Soc.* **2000**, *220*, U277–U277.
- (51) Jorgensen, W. L.; Tirado-Rives, J. The Opls Potential Functions for Proteins. Energy Minimizations for Crystals of Cyclic Peptides and Crambin. *J. Am. Chem. Soc.* **1988**, *110*, 1657–1666.
- (52) Kaminski, G. A.; Friesner, R. A.; Tirado-Rives, J.; Jorgensen, W. L. OPLS-AA/L Force Field for Proteins: Using Accurate Quantum Mechanical Data. *Abstr. Pap. Am. Chem. Soc.* **2000**, *220*, U279–U279.
- (53) Jorgensen, W. L.; Chandrasekhar, J.; Madura, J. D.; Impey, R. W.; Klein, M. L. Comparison of Simple Potential Functions for Simulating Liquid Water. *J. Chem. Phys.* **1983**, *79*, 926–935.
- (54) Mesleh, M. F.; Hunter, J. M.; Shvartsburg, A. A.; Schatz, G. C.; Jarrold, M. F. Structural Information from Ion Mobility Measurements: Effects of the Long Range Potential. *J. Phys. Chem. A* **1996**, *100*, 16082–16086.
- (55) Shvartsburg, A. A.; Jarrold, M. F. An Exact Hard-Spheres Scattering Model for the Mobilities of Polyatomic Ions. *Chem. Phys. Lett.* **1996**, *261*, 86–91.
- (56) Bleiholder, C.; Dupuis, N. F.; Wyttenbach, T.; Bowers, M. T. Ion Mobility-Mass Spectrometry Reveals a Conformational Con-

version from Random Assembly to  $\beta$ -Sheet in Amyloid Fibril Formation. *Nat. Chem.* **2011**, *3*, 172–177.

(57) Sugita, Y.; Okamoto, Y. Replica-Exchange Molecular Dynamics Method for Protein Folding. *Chem. Phys. Lett.* **1999**, *314*, 141–151.

(58) Anderson, S. E.; Bleiholder, C.; Brocker, E. R.; Stang, P. J.; Bowers, M. T.; Novel, A. Projection Approximation Algorithm for the Fast and Accurate Computation of Molecular Collision Cross Sections (III): Application to Supramolecular Coordination-Driven Assemblies with Complex Shapes. *Int. J. Mass. Spectrom.* **2012**, *330*, 78–84.

(59) Bleiholder, C.; Contreras, S.; Bowers, M. T.; Novel, A. Projection Approximation Algorithm for the Fast and Accurate Computation of Molecular Collision Cross Sections (IV). Application to Polypeptides. *Int. J. Mass. Spectrom.* **2013**, *354*, 275–280.

(60) Wiltzus, J. J. W.; Landau, M.; Nelson, R.; Sawaya, M. R.; Apostol, M. I.; Goldschmidt, L.; Soriaga, A. B.; Cascio, D.; Rajashankar, K.; Eisenberg, D. Molecular Mechanisms for Protein-Encoded Inheritance. *Nat. Struct. Mol. Biol.* **2009**, *16*, U973–U998.

(61) Do, T. D.; LaPointe, N. E.; Sangwan, S.; Teplow, D. B.; Feinstein, S. C.; Sawaya, M. R.; Eisenberg, D. S.; Bowers, M. T. Factors That Drive Peptide Assembly from Native to Amyloid Structures: Experimental and Theoretical Analysis of [Leu-5]-Enkephalin Mutants. *J. Phys. Chem. B* **2014**, *118*, 7247–7256.

(62) Maeda, S.; Sahara, N.; Saito, Y.; Murayama, M.; Yoshiike, Y.; Kim, H.; Miyasaka, T.; Murayama, S.; Ikai, A.; Takashima, A. Granular Tau Oligomers as Intermediates of Tau Filaments. *Biochemistry* **2007**, *46*, 3856–3861.